JJMIE

Volume 14, Number 4, December. 2020
ISSN 1995-6665
Pages 361 - 370

Jordan Journal of Mechanical and Industrial Engineering

MFL Based Prototype and Experimental Work for Detection of Defects in Cables of Bridge Structures

Emad Abdelsalam[a*], Feras Kafiah[a], Sanad Kiswani[a], Dana Ibrahim[a], Al Ghorbanpoor[b]

[a] School of Engineering Technology, Al Hussein Technical University, Amman 11831, Jordan
[b] Civil & Environmental Engineering Department, 3200 North Cramer Street, Milwaukee, WI 53211, USA

Received May 10 2020 Accepted November 3 2020

Abstract

This work offers experimental work and a prototype device based on the Magnetic Flux Leakage (MFL) method to inspect and detect corrosion in the cables of cable-stayed bridges. The developed prototype was constructed from two flat permanent magnets to provide a uniform magnetic field. A Hall-effect assembly was designed and developed. The assembly was placed between the two magnets in order to detect magnetic field changes due to defects inside the cable. Experimental work and tests were conducted on a constructed real cable, with various size of fabricated defect sizes. The results show that the MFL method is capable of detecting loss of section due to corrosion defects of varying sizes. Considerable success has been achieved in detecting steel defects from a single broken wire to seven broken wires (full strand fracture), particularly at the surface of the steel (about 3.8 cm depth from the surface of the cable). However, limited success has been achieved in detecting defects at the center of the steel cable, limited to detecting the seven broken wires defect only.

Keywords: NDE; Cable-Stayed Bridges; MFL; Corrosion;

1. Introduction

In the last seventy five years, a large number of bridges have been built in the United States and around the world. A majority of these bridge structures rely on stressed steel cables to carry all relevant loads from traffic, environmental effects, such as wind and temperature, earthquakes, and the weight of the structure. Over time, these bridges age and become exposed to environmental conditions, such as rain, snow, de-icing and harmful chemicals. These conditions cause various levels of deterioration in the steel, particularly corrosion. Having said that, corrosion causes a loss of cross-section in the steel, adversely affecting the bridge's capacity to carry its service loads, and can possibly place the bridge's performance and safety in a critical condition. Several cases of post-tensioned (P-T) cable corrosion in bridges have been reported throughout the world. For example, in the summer of 1999, Florida Department of Transportation (FDOT) discovered corrosion in multiple bridges including the Niles Channel Bridge in the Florida Keys. Also, in 2000, a fractured tendon and advanced stages of corrosion in the cable anchorage area were observed during a routine bridge inspection by FDOT at the Mid-bay Bridge near Destin. Moreover, similar problems have been discovered at the Skyway Bridge in Tampa, FL [1]. Also, bridge collapses due to excessive corrosion have been reported in the United States and in other parts of the world [2]–[7]. According to the above, there is a direct need for developing appropriate inspection methods to effectively detect corrosion in bridge cables and evaluate the structural integrity, performance and safety of such structures. While different defects are formed in various structural members in bridge structures, the focus of this work is placed on the corrosion problems in primary steel cables of large bridges. Such cables are normally enclosed in protective polyethylene, metallic ducts or wrapping materials to prevent exposure to moisture and outside environment. As such, no visual evaluation is possible and there have been no practical commercial technologies that could be used to evaluate the condition of these bridge cables. There are many NDE methods such as X-ray, Ultrasound, Electrical Resistance gages, Time Domain Reflectometry, Linear Polarization, vibration techniques, Surface Potential Survey and Themography that may be applicable for bridge cables inspection [8]–[28]. Although these NDE methods may offer some evaluation capabilities for bridge cables, it has been shown that they are ineffective in the detection of corrosion in bridge cables [10]–[19], [21]–[46]. However, the MFL concept has been successfully demonstrated to be effective in detecting defects such as loss of section and corrosion in external P-T ducts of concrete bridge structures [37], [43]–[52]. Based on the literature survey, it was found that only the MFL method can offer both the performance required to detect corrosion in bridge steel cables and the effectiveness for field applications [37], [43]–[46]. This work presents development and laboratory evaluation of an MFL system that is capable of inspecting and detecting steel corrosion in cable supported bridge structures. The work is part of our

* Corresponding author e-mail: Emad.Abdelsalam@htu.edu.jo.

proposed NDE system that combines MFL and Magnetostrictive techniques [53]. The MFL prototype and experimental work laid the ground for the feasibility of combining the Magnetostrictive and the MFL method to develop a comprehensive system that is not only capable of inspecting the entire length of the cable of the cable-stayed bridge, but also the anchorage area. Such system is not commercially available. There are systems in the market that use MFL, mostly cylindrical magnet with sensors [47], that can be mounted on the cable, but cannot inspect the anchorage area.

2. Theory and Concept

The basic principle behind the MFL method is to apply a magnetic field near the surface of the steel cable and monitor the variation of the magnetic flux in the cable. The magnetic field must be strong enough to adequately penetrate through the steel cable. Since steel is a ferromagnetic material, magnetic flux will flow through the steel and be confined within the steel structure, Figure 1. However, if there is a deficiency in the physical structure of the steel, such as a loss of cross section due to corrosion or fracture, the magnetic flux will leak to the surrounding environment, Figure 1b. This is referred to as "magnetic fringing" phenomenon. To take advantage of this phenomenon, magnetic sensors, like Hall-effect, are placed near the surface of the cable where an electrical signal can be observed and recorded in the form of voltage variations due to magnetic fringing. This signal, which is an indication of the presence of the flaw, can then be used to evaluate the severity of the deterioration. The magnitude and duration of the signal varies based on several factors, including the depth, size and shape of the defect in the steel cable.

The flux leakage is dependent on the size of the flaw, strength of the magnetic field, and the distance between the flaw and magnetic sensor. The stronger the magnetic field, the more the leakage of the flux lines. Similarly, the larger the flaw is, the more leakage of the magnetic field. Figure 2 demonstrates the concept of MFL and the effect of magnetic field strength on the density of leakage flux.

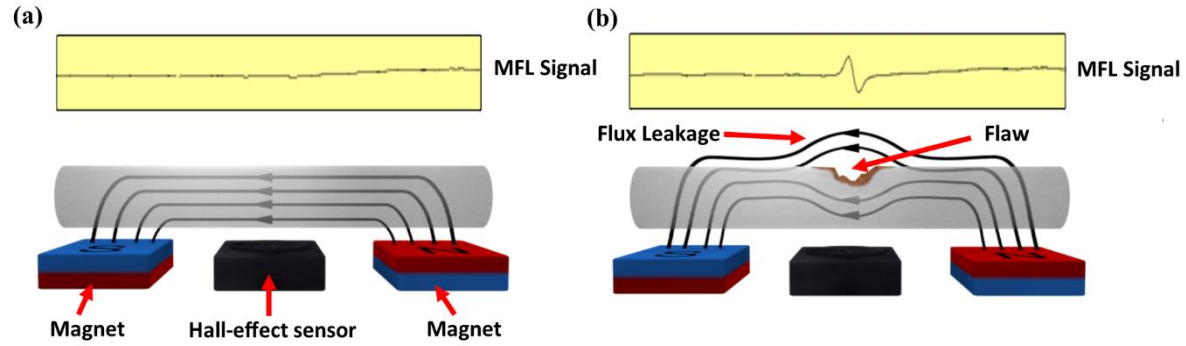

Figure 1. Demonstrating MFL concept: (a) without flaw in a steel bar, (b) with a flaw in a steel bar.

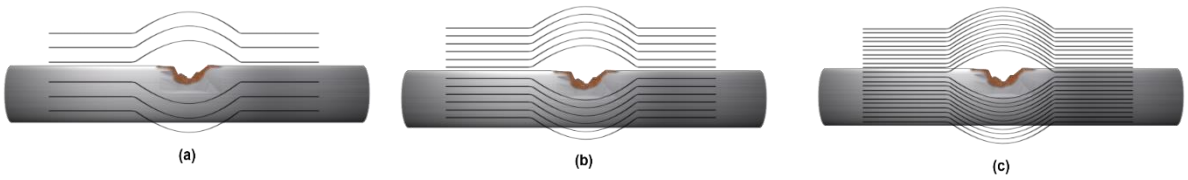

Figure 2. Effect magnetic field strength on the density of induced flux lines. (a) Low magnetic field, (b) Medium magnetic field and (c) Strong magnetic field.

2.1. Mathematical Model

The MFL technique has been widely used in NDE for detecting metal-loss due to corrosion or fatigue cracking problems in steel structures, particularly for inspecting oil and gas pipelines. The usage of the MFL technique to inspect gas pipelines goes back to early 1960's [54]–[64]. Similar to other NDE techniques, the interest when using the MFL method is to be able to predict the characteristics (size and shape) of the defect by solving the inverse problem of the signal output recorded from MFL sensors. As such, many methods have been attempted to solve the inverse problem solution; these can be classified as model or non-model based methods. The model-based (numerical) methods use a physical model to solve the inverse problem. These methods rely on iterative and optimized loops to find the solution for the inverse problem based on an initial guess or prior knowledge of the MFL defect parameters. These methods rely on numerical models [58]–[60], such as finite element method (FEM), analytical models [61]–[63], [65] and neural networks [55], [56], [64]. Although numerical methods provide an accurate solution for the inverse problem, they are computationally expensive. Corrosion characteristics [66] and estimation of defect severity [67] were studied. On the other hand, analytical and neural network methods are less accurate due to the approximation made to drive them, but they are faster methods [68]. The non-model based methods use signal processing techniques to correlate the signal from the MFL sensor to the shape of the defect. For example, the neural network method is used to train the model to predict the shape of the MFL signal based on prior knowledge. However, the model is usually limited to a specific region in the defect and is difficult to apply to an arbitrary shape defect [68]. Other methods combine the accuracy of the FEM methods with the efficiency of the analytical methods using space mapping (SM) [69]–[74]. In the recent work [68], edge detection method is used to predict the shape of the flaw from the top, while using SM methods to estimate the depth parameter for an arbitrary defect. Also, other methods [75] have been proposed for the mathematical models of MFL defects based on the type of defect. Metal loss defects are classified as surface and sub-surface defects. For surface defects, the focus of the work was to develop an analytical model for a slot-type defect. As such, different models have been proposed which include Förster [76], Zatsepin and Shcherbinin [77], [78]. For sub-surface defects, the work was focused on two particular types of defects, cylindrical and spherical. The steel used in cable-stayed bridges is a bundle of either straight wires or strands; each strand consisting of a certain number of individual twisted wires, as shown in Figure 3. Although defects can be of any shape, it is reasonable to consider fractured wires as a target defect for our work following the same approach and consideration for similar types of research. As such, a broken wire is best represented by cylindrical sub-surface flaw, as seen in Figure 4. The mathematical model for a sub-surface cylindrical flaw, has been developed by Swartzendruber [79].

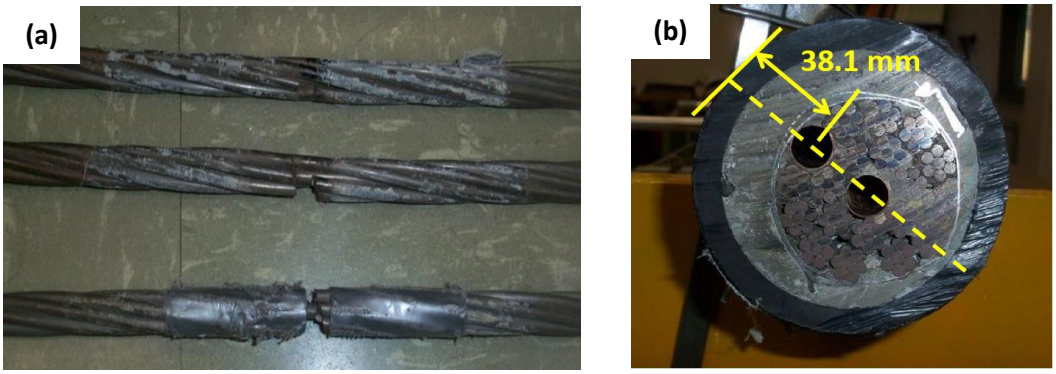

Figure 3. (a) Typical steel strands with a bundle of wires used in cable-stayed bridge; showing man-made defects, from top to bottom, of one broken wire, two broken wires and five broken wires. (b) Cable showing bundle of steel wires/strands with concrete grout and protective cover.

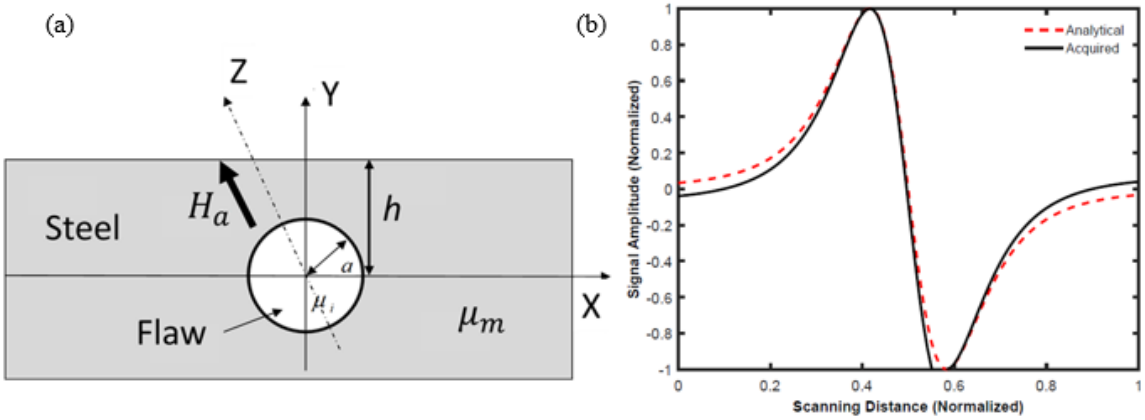

Figure 4: (a) MFL Mathematical Model: Illustration of sub-surface cylindrical flaw. (b) Acquired MFL signal and predicated signal based on the mathematical model in equation (2).

The analytical model for the magnitude of the flux leakage for a sub-surface cylindrical flaw of a radius ***a*** and depth ***h*** can be described with the following equation [79]:

$$m = \frac{2\mu_m}{\mu_m + \mu_i}\left[1 - \left(\frac{\mu_m - \mu_i}{\mu_m + \mu_i}\right)^2 \left(\frac{a}{2h}\right)^2\right]^{-1} \frac{\mu_m - \mu_i}{\mu_m + \mu_i} H_a\, a^2 \quad (1)$$

$$H_y = \frac{2xy}{(x^2 + y^2)^2}\,(m - 2H_a\, a^2) \quad (2)$$

$$H_x = \frac{(x^2 - y^2)}{(x^2 + y^2)^2}\,(m - 2H_a\, a^2) \quad (3)$$

Where,

μ_m is permeability of the material under test; μ_i is permeability of the cylindrical defect; h is the depth of the flaw; a radius of the flaw; H_a is the applied magnetic field; H_x is the horizontal component of the magnetic field; H_y is the vertical component of the magnetic field.

The mathematical model stated above represents the flux leakage for a sub-surface cylindrical defect in a two-dimensional form. Figure 4 shows a comparison between a real magnetic flux leakage flaw signal from a test and that from the mathematical model of equation (2). The figure demonstrates that there is a good agreement between the signals from the real flaw and the mathematical model. The mathematical model shown above represents the flux leakage for a sub-surface cylindrical flaw in 2D only and it does not relate to the length of the flaw.

3. System Prototype

The MFL system developed consists of two strong permanent magnets as shown in Figure 5 (a). Each magnet is polarized perpendicular to its surface where the flux lines travel from the north-pole surface of the first magnet to the south-pole surface of the second magnet. The pair of magnets is polarized opposite to each other to allow the flux lines to travel from one magnet to the other, creating a uniform magnetic field between the two magnets. The permanent magnets selected for the MFL system are two large Neodymium Iron Boron magnets that have a strength of approximately 2,200 gauss at the center of each piece. Each one of the two magnets is a packed assembly of eight individual magnets of approximately 50 mm x 50 mm x 38 mm that are housed in a sealed stainless steel enclosure. The overall dimension of each magnet with the enclosure is approximately 210 mm x 108 mm x 46 mm. The weight of each magnet is approximately 6.2 kg. Each magnet's dimensions and layout have been optimized to provide a uniform magnetic field and maximum field penetration (50 to 75 mm from the surface of the cable) within the desired limits of detection for loss of section in bridge cables. A Hall-effect sensor enclosure that includes an array of ten Hall-effect sensors and a series of signal amplifiers have been placed between the two magnets. The Hall-effect sensors are placed at the isocenter of the two magnets to assure symmetry for the resultant MFL flaw signals. The Hall-effect sensors used in this MFL system are surface sensors and arranged to capture only the vertical component of the magnetic field leakage. The Hall-effect sensors are arranged in one array that consists of seven sensors. The lateral distance between each two adjacent sensors is kept at 25.4 mm. The sensors are arranged on a printed electrical circuit board along with electrical signal conditioning (amplification and filtration) hardware. The entire magnet and sensor assembly is mounted on an aluminum frame with wheels to allow moving the magnet on the surface of the cable. An encoder device is attached to one end of the frame to allow tracking of the position of the scan and subsequently it is used to identify the location of defects. The output of the sensors is connected to a data acquisition device. The data from sensors is collected and displayed in real time on a laptop computer using the LabVIEW software from the National Instrument Company (NI). The software has been designed to allow continuous display of data from all ten sensors simultaneously or from selected sensors only. Further post processing software application has been created to allow for data analysis.

4. Results and Discussion

To demonstrate the capabilities and effectiveness of the MFL system, several laboratory experiments were conducted. A 114.3 mm diameter bridge cable of 2.43 m long, which is similar to the commonly used bridge cables was used in the laboratory. The bridge cable consists of a bundle of 19 strands, as seen in Figure 3 (b). Two strands, one at the edge and one at the center of the strand bundle, were replaced by two copper tubes to allow insertion of strands with pre-set flaws in the laboratory bridge cable. Several defect sizes, from a single wire fracture to a complete strand fracture, were fabricated and inserted, one at a time, in the copper tube., Figure 5c. The magnet assembly was first mounted on top of the laboratory bridge cable and connected to the data acquisition software. The magnet assembly was then moved to a known starting point on the cable to establish a reference point for the start of the scan. The experiments were carried out by inserting a strand, with known flaws, into the top or the outer copper tube (25.4 mm) in the cable. The first inserted strand contained seven broken wires (complete strand fracture).

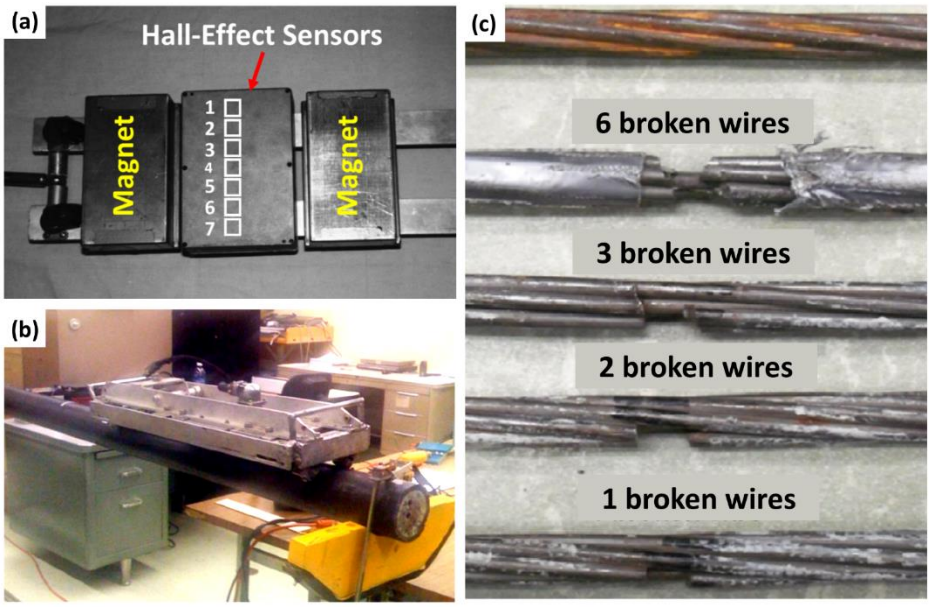

Figure 5. (a) The MFL system with two permanent magnets and a sensor enclosure (sensors 1 through 7) in the middle [37], [43]–[46] (b) MFL system installed on a laboratory bridge cable; showing 19 strands cable, with two strands inserted in the top and center holes in the cable. (c) Prestressing steel strands with no flaws (top) and with different sizes of flaws.

The strand was inserted inside the copper tube until it reached a predetermined length for the location of the flaw. The cable was scanned with the magnet assembly manually along the length of the cable in searching for flaws. The magnet assembly was moved as it passed the location of the flaw, and then stopped at the end of the cable. When the magnet reached at the end of the cable, data acquisition was stopped and the magnet was moved back to the start point, ready for the next scan. Data was collected continuously during each scan and it was transferred to the computer where it was saved for post-processing. The data from the seven Hall-effect sensors were collected and viewed in real-time while scanning the cable. When the first test was completed, the strand was removed and the second strand, with six broken wires, was inserted in the cable hole. Similar to the first scan, the magnet was moved over the flaw starting at the beginning of the cable from the same reference point and ending at the end of the cable moving exactly the same distance. The rest of the scanning was performed similarly for the remaining strands with varying defect sizes. When this part of the testing was completed, the first strand (with seven broken wires) was inserted in the center copper tube (located at 63.5 mm of depth) in the cable. The strand was pushed inside the cable until it reached the predetermined flaw location, similar to the first experiment, to maintain consistent location of the flaw within the cable.

4.1. Effect of seven broken wires at 38.1 mm depth inside the cable

The results of the first scan (seven broken wires in the outer copper tube) are shown in Figure 6. The x-axis of the graph represents the distance the magnet travelled during the scan. The y-axis represents the amplitude of the magnetic flux that leaked outside the steel. The graph shows only the vertical component of the magnetic flux; the flat line in the graph indicates that there is no flux leakage. Any variations in the graph indicate the presence of a local disturbance of the magnetic field, and possibly an indication of the loss of section or presence of a flaw. The graphs clearly show strong variations based on the magnitude of the signal amplitude indicating the presence of disturbances near that area. Also, the data show that the signals recorded from all seven Hall-effect sensors vary in magnitude based on the location of each sensor. The maximum peak-to-peak magnitude (0.9 $V_{pk\text{-}pk}$) is observed at sensor four which is the closest sensor to the flaw. Additionally, the graph shows that the signal amplitude decreases from all other sensors as they are further away from the location of the flaw.

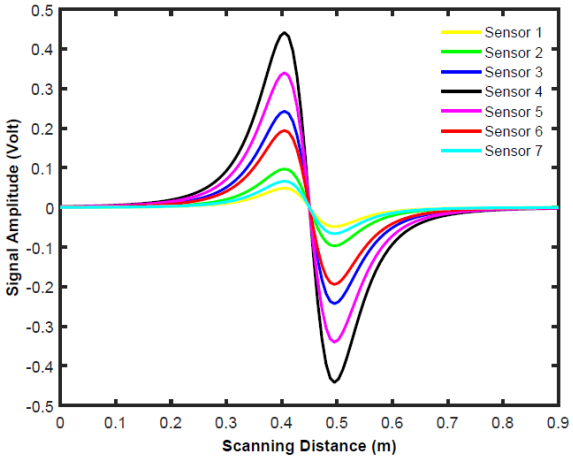

Figure 6. MFL signals recorded from sensors 1 through 7 for seven broken wires. Larger signal amplitude values are resulted from sensors that are located closer to the defects, i.e., data from sensors 4 and 5.

4.2. Effect of six broken wires at 38.1 mm depth inside the cable

In this experiment, the strand with seven broken wires was removed and a strand with six broken wires was

inserted in the top copper tube in the cable. Similar to the first scan, the magnet was moved over the flaw location traveling exactly the same distance on the cable. The signals recorded for the defects of the six broken wire-strand are shown in Figure 7. The signals from all seven sensors are almost identical to the defect signals of the seven-broken-wire strand, except that the peak-to-peak signal amplitude is lower. The data shows that the maximum signal amplitude recorded is about 0.8 V_{pk-pk}; which corresponds to sensor four, as expected. The data also show that sensors 3 and 5 produced the next highest signal amplitude levels when compared to the signals from sensor four. It is also clear from the graphs that the signal from sensor one is the smallest since it is the farthest from the location of the defect.

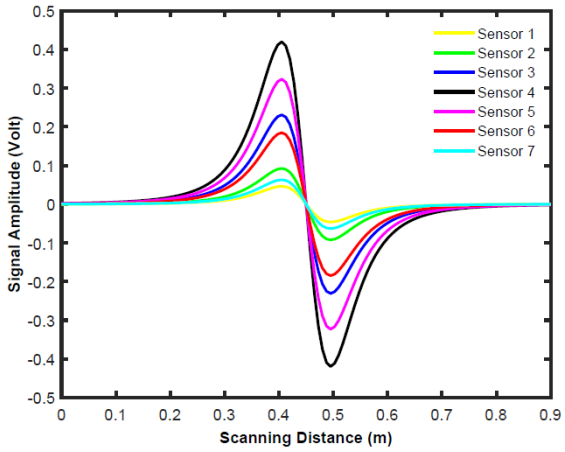

Figure 7. MFL signals recorded from sensors 1 through 7 for six broken wires. Larger signal amplitude values are resulted from sensors that are located closer to the defects, i.e., data from sensors 4 and 5.

4.3. Effect of five broken wires at 38.1 mm depth inside the cable

In this experiment, the strand with six broken wires was removed and a strand with five broken wires was inserted in the outer copper tube in the cable. The data for the defect of the five broken wires in the strand is shown in Figure 8. Consistent with the previous two experiments for 7-wires and 6-wires broken strands, the maximum signal is recorded from sensor four. As seen from the graph, the peak-to-peak magnitude of the signal for sensors four is about 0.7 V_{pk-pk}. The signals from the rest of the sensors follow the pattern as in the previous two experiments, where sensor one shows the smallest magnitude.

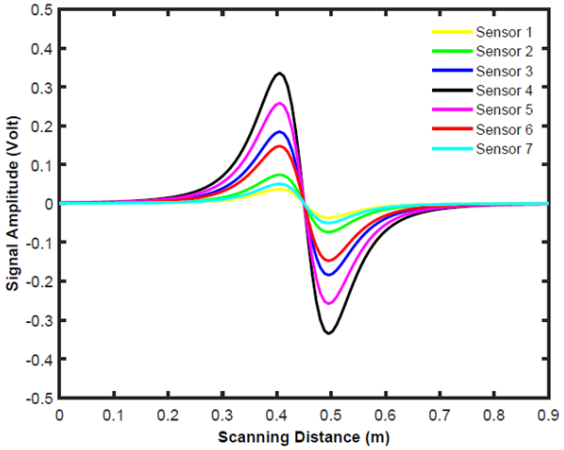

Figure 8. MFL signals recorded from sensors 1 through 7 for five broken wires. Larger signal amplitude values are resulted from sensors that are located closer to the defects, i.e., data from sensors 4 and 5.

4.4. Effect of four broken wires at 38.1 mm depth inside the cable

In this experiment, the strand with five-broken-wires was removed and a strand with four broken wires was inserted in the outer copper tube in the cable. The data is shown in Figure 9. Consistent with the previous results, the maximum signal is recorded from sensor four with 0.5 V_{pk-pk}. The signals from the rest of the sensors follow the pattern as in the previous experiments, where, sensor one shows the smallest magnitude.

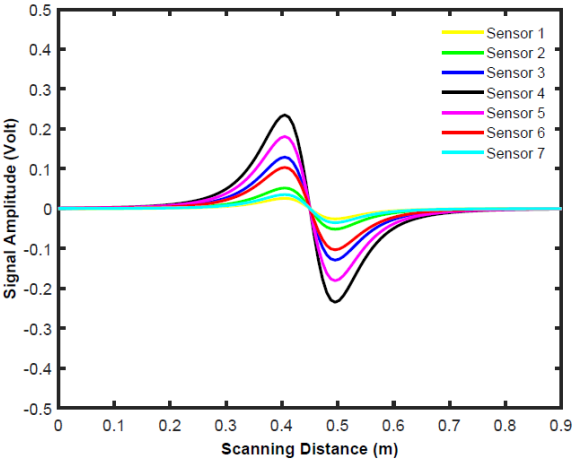

Figure 9. MFL signals recorded from sensors 1 through 7 for four broken wires. Larger signal amplitude values are resulted from sensors that are located closer to the defects, i.e., data from sensors 4 and 5.

4.5. Effect of three broken wires at 38.1 mm depth inside the cable

The data for the defect in a strand with three broken wires are shown in Figure 10. As seen from the graph, the peak-to-peak magnitude of the signal for sensor four about 0.35 V_{pk-pk}. The signals from the rest of the sensors follow the pattern as in the previous experiments, where, sensor one shows the smallest magnitude.

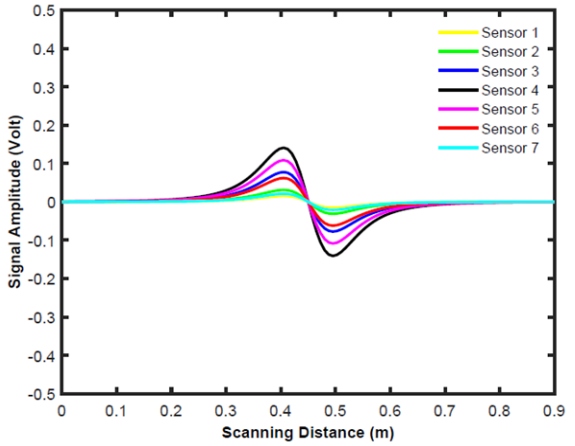

Figure 10. MFL signals recorded from sensors 1 through 7 for three broken wires. Larger signal amplitude values are resulted from sensors that are located closer to the defects, i.e., data from sensors 4 and 5.

4.6. Effect of two broken wires at 38.1 mm depth inside the cable

The data for the defects for the two broken wires strand is shown in Figure 11. As seen from the graph, the peak-to-peak magnitude of the signals from sensor four is almost about 0.15 V_{pk-pk}. The signals from the rest of the sensors follow the pattern as in the previous experiments, where, sensor one shows the smallest magnitude.

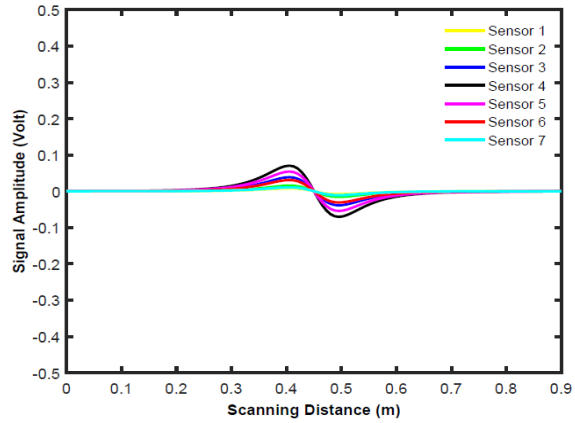

Figure 11. MFL signals recorded from sensors 1 through 7 for two broken wires. Larger signal amplitude values are resulted from sensors that are located closer to the defects, i.e., data from sensors 4 and 5.

4.7. Effect of one broken wire at 38.1 mm depth inside the cable

In the last experiment, a strand with one broken wire defect was inserted in the outer copper tube in the cable. The results for this experiment are shown in Figure 12. As seen from the graph, the peak-to-peak magnitude of the signal for sensor four is about 0.075 V_{pk-pk}.

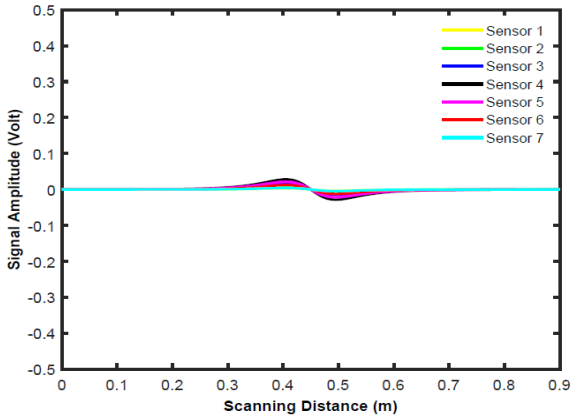

Figure 12. MFL signals recorded from sensors 1 through 7 for one broken wire. Larger signal amplitude values are resulted from sensors that are located closer to the defects, i.e., data from sensors 4 and 5.

The results of the experiments are summarized in Figure 13. The graph shows that the MFL system offers good response and sensitivity to the size of flaws varying from 1-broken wire to 7-broken wires in a strand. The experiments were carried out on single isolated defects (defects that are far from each other). However, when defects were very close to each other, it was difficult to visually distinguish the MFL signal for each individual defect. For example, the presence of a large defect next to relatively small defect may mask the signal from the small defect, which may alter the shape of the signal of the large defect. This may suggest the need for more sophisticated signal processing or pattern recognition techniques to improve defect detectability. Additionally, the developed prototype model is a rectangular magnet, it can only cover a section of the diameter of the cable. Hence, rotating the magnet around the diameter of the cable and rescanning is necessary to ensure full coverage of the diameter of the cable. However, this is not practical and is time consuming. Furthermore, keeping the magnet in a straight-line during scanning along the length of the cable is another practical challenge. Hence, motion alignment, tracking and adjustment are necessary. Installing the device on the cable is also another practical problem, as the magnet is very strong and can easily pull towards the cable quickly due to the magnetic force.

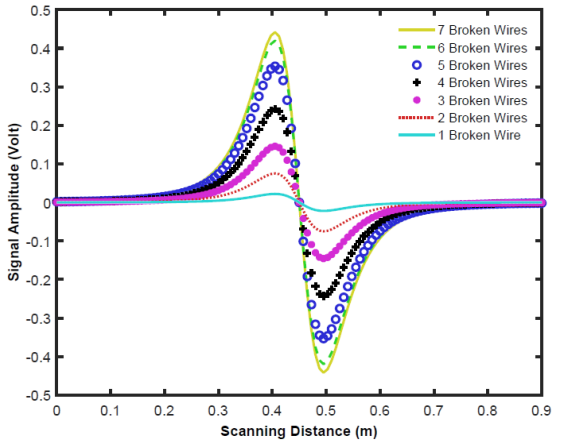

Figure 13. Summary of MFL signals recorded from sensors four for one broken wires to seven broken wires.

5. Conclusion

The use of MFL method has been studied and evaluated for detecting section losses in the bridge cables through experimental work. A prototype model of the MFL system has been used. Also, data acquisition hardware for signal amplification and conditioning has been developed. Furthermore, data acquisition software for real-time acquisition and post-processing analysis has been developed. A grouted 127 mm diameter bridge cable that consists of pre-stressing strands has been used for the MFL experiments to evaluate the system performance. The results have shown that the MFL technique is capable of detecting corrosion-related defects (section loss) inside the cable. These include a single broken wire within one strand to several broken wires with considerable success if the location of the flaw is within about 38.1 mm from the surface of the cable. However, successful section loss detection at the center of the steel cable has been limited to seven broken wires. The current MFL system built based on a flat rectangular magnets can only cover a portion of the circumference of the cable. As such, it is necessary to rotate the magnets around the cable and repeat the scans for the entire length of the cable several times to cover the full volume of the cable. This is not practical in the field, especially for long span bridges where the length of each bridge cable may exceed 426 m. To address this limitation, a new design based on cylindrical magnets can be proposed for future work.

References

[1] Florida Department of Transportation (FDOT) Report, "Post-tensioned Bridges, Topic No. 700-000-000, Section 10.7," 2004.

[2] A. G. Lichtenstein, "The silver bridge collapse recounted," *J. Perform. Constr. Facil.*, vol. 7, no. 4, pp. 249–261, 1993.

[3] K. P. Chong, N. J. Carino, and G. Washer, "Health monitoring of civil infrastructures," *Smart Mater. Struct.*, vol. 12, no. 3, p. 483, 2003.

[4] D. Appell, "Repairs without rivets.," *Sci. Am.*, vol. 297, no. 5, pp. 21–22, 2007.

[5] R. J. Woodward and F. W. Williams, "COLLAPSE OF YNS-Y-GWAS BRIDGE, GLAMORGAN.," *Proc. Inst. Civ. Eng.*, vol. 84, no. 4, pp. 635–669, 1988.

[6] D. Parker, "Pacific bridge collapse throws up doubt on repair method," *New Civ. Eng.*, vol. 12, pp. 12–96, 1996.

[7] D. Parker, "Tropical overload," *New Civ. Eng.*, pp. 18–21, 1996.

[8] D. E. Bray and R. K. Stanley, *Nondestructive evaluation: a tool in design, manufacturing and service*. CRC press, 1996.

[9] P. J. Shull and C. R. C. Press, "Nondestructive Evaluation Theory, Techniques and Applications,(2002)." Marcel Dekker.

[10] J. L. Robert and M. Brachet-Rolland, "Survey of structures by using acoustic emission monitoring," *IABSE REPORTS*, vol. 39, 1982.

[11] M. Schupack, "Evaluation of Corrosion in Bonded and Unbonded Post-Tensioned Structures. How to make Today's Repairs Durable for Tomorrow," Houston, Texas, 1998.

[12] S. Feliu, J. A. Gonzalez, C. Andrade, and I. Rz-Maribona, "Errors Introduced by the Guard Ring Device in the On-Site Measurement of Rebar Corrosion Rates. Corrosion of Reinforcement in Concrete. Papers Presented at the Third International Symposium On" Corrosion of Reinforcement in Concrete Construction", Belfry ," *Publ. CICC Publ.*, pp. 293–302, 1990.

[13] D. G. John and D. Eden, "Corrosion measurements on reinforcing steel and monitoring of concrete structures," *Corros. Met. Concr.*, pp. 159–167, 1987.

[14] W. K. Green, S. B. Lyon, and J. D. Scantlebury, "Electrochemical changes in chloride-contaminated reinforced concrete following cathodic polarisation," *Corros. Sci.*, vol. 35, no. 5–8, pp. 1627–1631, 1993.

[15] R. H. Suresh Bapu, N. U. Nayak, C. Srividya Rajagopalan, S. Srinivasan, N. S. Rengaswamy, and Y. Mahadeva Iyer, "Monitoring of corrosion of prestressing steel cables in prestressed concrete bridges," *Trans. SAEST*, vol. 23, no. 2–3, pp. 203–206, 1988.

[16] American Society for Testing Materials, "Standard Test Method for Half-Cell Potentials of Reinforcing in Concrete."

[17] C. C. Naish, A. Harker, and R. F. A. Carney, "Concrete inspection: interpretation of potential and resistivity measurements," *CICC Publ. - Corros. Reinf. Concr.*, pp. 314–332, 1990.

[18] E. Escalante, "Effectiveness of potential measurements for estimating corrosion of steel in concrete," *Elsevier Appl. Sci.*, pp. 281–292, 1990.

[19] D. J. Daniels, "Surface-penetrating radar," *Electron. Commun. Eng. J.*, vol. 8, no. 4, 1996.

[20] C. Hellier, *Handbook of Nondestructive Evaluation*, 2001st ed. McGraw-Hill Education, 2001.

[21] N. J. Carino, "The impact-echo method: an overview," in *Structures 2001: A Structural Engineering Odyssey*, 2001, pp. 1–18.

[22] H. E. Martz, D. J. Scheberk, G. P. Roberson, and P. J. M. Monteiro, "Computerized tomography analysis of reinforced concrete," *Mater. J.*, vol. 90, no. 3, pp. 259–264, 1993.

[23] C. Flohrer and B. Bernhardt, "Detection of Prestressed Steel Tendons Behind Reinforcement Bars, Detection of Voids in Concrete Structures - A Suitable Application for Radar Systems," in *Conference Proceedings of The British Institute of Non-Destructive Testing International Conference, NDT in Civil Engineering 14-16 April 1993, Liverpool University. Volume 1*, 1992, pp. 227–237.

[24] C.-C. Cheng and M. Sansalone, "Effects on impact-echo signals caused by steel reinforcing bars and voids around bars," *Mater. J.*, vol. 90, no. 5, pp. 421–434, 1993.

[25] Y. Lin and M. Sansolone, "Detecting flaws in concrete beams and columns using the impact-echo method," *Mater. J.*, vol. 89, no. 4, pp. 394–405, 1992.

[26] D. Pratt and M. Sansalone, "Impact-echo signal interpretation using artificial intelligence," *Mater. J.*, vol. 89, no. 2, pp. 178–187, 1992.

[27] N. J. Carino and M. Sansalone, "Detection of voids in grouted ducts using the impact-echo method," *Mater. J.*, vol. 89, no. 3, pp. 296–303, 1992.

[28] C. G. Petersen, "DOCter impact echo testing of the injection of a post-tensioned cable steel duct "," *Report-German Instruments A/S*, 1993.

[29] M. G. Ali and A. R. Maddocks, "Evaluation of corrosion of prestressing steel in concrete using non-destructive techniques," *Non-Destructive Testing-Australia*, vol. 40, no. 5, pp. 42–48, 2003.

[30] M. B. Leeming, J. S. Lane, and P. J. Wade, "Post-tensioned bridge investigation-the way forward," in *Proceedings of the sixth international conference on structural faults and repair*, 1995, pp. 193–197.

[31] R. T. Stain, "Dixon, 5,—Inspection of cables in post-tensioning bridge-What techniques are available "," *Construction/Repair*, pp. 297–300, 1994.

[32] H. T. Williams and M. E. Hulse, "From theory to experience with inspection of post-tensioned bridges," in *Proc., 6th Int.*

Conf. on Structural Faults and Repairs, 1995, vol. 1, pp. 199–202.

[33] M. Nagi and D. Whiting, "Corrosion of prestressed reinforcing steel in concrete bridges: State-of-the-art," *Spec. Publ.*, vol. 151, pp. 17–42, 1994.

[34] ANON, "Inspection of Prestressing Cables in Bridges," *Indian Concr. J.*, vol. 61, no. 2, pp. 31–33, 1987.

[35] O. Büyüköztürk, "Imaging of concrete structures," *Ndt E Int.*, vol. 31, no. 4, pp. 233–243, 1998.

[36] W. I. J. Price, "Highway Bridge Inspection: Principles And Practices In Europe," *IABSE REPORTS*, vol. 38, 1982.

[37] G. R. Steber, A. Ghorbanpoor, and T. E. Shew, "Magnetic field disturbance signal processing," in *15th Annual Conference of IEEE Industrial Electronics Society*, 1989, pp. 474–479.

[38] A. Ghorbanpoor and T. E. Shew, "Detection of flaws in bars and cables in concrete bridge structures," *Transp. Res. Rec.*, no. 1211, pp. 84–91, 1989.

[39] B. Gimmel, "Magnetoelastic Force Measurement in Prestressed Concrete," in *Durability of Structures. IABSE Symposium, September 6-8 1989, Lisbon (IABSE Report Volume 57/1)*, 1989, pp. 239–334.

[40] H. Scheel and B. Hillemeier, "Capacity of the remanent magnetism method to detect fractures of steel in tendons embedded in prestressed concrete," *NDT E Int.*, vol. 30, no. 4, pp. 211–216, 1997.

[41] M. G. Fontana, *Corrosion engineering*. Tata McGraw-Hill Education, 2005.

[42] M. Huang, L. Jiang, P. K. Liaw, C. R. Brooks, R. Seeley, and D. L. Klarstrom, "Using acoustic emission in fatigue and fracture materials research," *JOM*, vol. 50, no. 11, pp. 1–14, 1998.

[43] A. Ghorbanpoor, R. Borchelt, M. Edwards, and E. A. Salam, "Magnetic-Based NDE of Prestressed and Post-Tensioned Concrete Members: The MFL System.," 2000.

[44] A. Ghorbanpoor, G. R. Steber, and T. E. Shew, *Evaluation of Steel in Concrete Bridges: The Magnetic Field Disturbance (MFD) System*. Federal Highway Administration, 1991.

[45] E. Abdelsalam, "Corrolation Analysis of Flaw Signal Detected by the MFD System," University of Wisconsin-Milwaukee, 1998.

[46] Engineering News-Record, "Magnetic Flux Leakage is Powerful New Force in Bridge Inspection," *Equip. Tracks Trends*, vol. 244, no. 11, p. 35, 2000.

[47] H. B. Yun, S. H. Kim, L. Wu, and J. J. Lee, "Development of inspection robots for bridge cables," *Sci. World J.*, vol. 2013, no. December, 2013, doi: 10.1155/2013/967508.

[48] Y. Ma, L. Lin, K. Jiang, and X. Zhao, "The application of magnetic shielding effect in drill pipe magnetic leakage flux testing," *Proc. - 2013 5th Conf. Meas. Technol. Mechatronics Autom. ICMTMA 2013*, no. 1, pp. 1135–1138, 2013, doi: 10.1109/ICMTMA.2013.277.

[49] K. Muramatsu, Y. Gao, Y. Moriyama, H. Dozono, T. Nishino, and K. Miura, "Modeling of Leakage Magnetic Field of Electric Machines Using Blocks with Magnetizations for Design of Magnetically Shielded Room," *IEEE Trans. Magn.*, vol. 53, no. 6, pp. 2015–2018, 2017, doi: 10.1109/TMAG.2017.2657639.

[50] A. Azad and N. Kim, "Design and optimization of an MFL coil sensor apparatus based on numerical survey," *Sensors (Switzerland)*, vol. 19, no. 22, 2019, doi: 10.3390/s19224869.

[51] K. Tsukada *et al.*, "Detection of Inner Corrosion of Steel Construction Using Magnetic Resistance Sensor and Magnetic Spectroscopy Analysis," *IEEE Trans. Magn.*, vol. 52, no. 7, pp. 1–4, 2016, doi: 10.1109/TMAG.2016.2530851.

[52] K. Tsukada *et al.*, "Detection of Inner Cracks in Thick Steel Plates Using Unsaturated AC Magnetic Flux Leakage Testing with a Magnetic Resistance Gradiometer," *IEEE Trans. Magn.*, vol. 53, no. 11, pp. 1–5, 2017, doi: 10.1109/TMAG.2017.2713880.

[53] A. Salam and E. Ismail, "System for Detection of Defects in Cables of Bridge Structures," 2013.

[54] S. R. H. Hoole, "Artificial neural networks in the solution of inverse electromagnetic field problems," *IEEE Trans. Magn.*, vol. 29, no. 2, pp. 1931–1934, 1993.

[55] P. Ramuhalli, L. Udpa, and S. Udpa, "Neural network algorithm for electromagnetic NDE signal inversion," *Electromagn. Nondestruct. Eval.*, pp. 121–128, 2001.

[56] P. Ramuhalli, L. Udpa, and S. S. Udpa, "Neural network-based inversion algorithms in magnetic flux leakage nondestructive evaluation," *J. Appl. Phys.*, vol. 93, no. 10, pp. 8274–8276, 2003.

[57] R. Schifini and A. C. Bruno, "Experimental verification of a finite element model used in a magnetic flux leakage inverse problem," *J. Phys. D. Appl. Phys.*, vol. 38, no. 12, pp. 1875–1880, 2005.

[58] Z. Chen, G. Preda, O. Mihalache, and K. Miya, "Reconstruction of crack shapes from the MFLT signals by using a rapid forward solver and an optimization approach," *IEEE Trans. Magn.*, vol. 38, no. 2, pp. 1025–1028, 2002.

[59] M. Yan, S. Udpa, S. Mandayam, Y. Sun, P. Sacks, and W. Lord, "Solution of inverse problems in electromagnetic NDE using finite element methods," *IEEE Trans. Magn.*, vol. 34, no. 5, pp. 2924–2927, 1998.

[60] C. Mandache and L. Clapham, "A model for magnetic flux leakage signal predictions," *J. Phys. D. Appl. Phys.*, vol. 36, no. 20, pp. 2427–2431, 2003.

[61] D. Minkov, J. Lee, and T. Shoji, "Study of crack inversions utilizing dipole model of a crack and Hall element measurements," *J. Magn. Magn. Mater.*, vol. 217, no. 1–3, pp. 207–215, 2000.

[62] C. Edwards and S. B. Palmer, "The magnetic leakage field of surface-breaking cracks," *J. Phys. D. Appl. Phys.*, vol. 19, no. 4, pp. 657–673, 1986.

[63] A. Joshi, L. Udpa, S. Udpa, and A. Tamburrino, "Adaptive wavelets for characterizing magnetic flux leakage signals from pipeline inspection," *IEEE Trans. Magn.*, vol. 42, no. 10, pp. 3168–3170, 2006.

[64] P. Ramuhalli, L. Udpa, and S. S. Udpa, "Electromagnetic NDE signal inversion by function-approximation neural networks," *IEEE Trans. Magn.*, vol. 38, no. 6, pp. 3633–3642, 2002.

[65] D. Minkov and T. Shoji, "Method for sizing of 3-D surface breaking flaws by leakage flux," *NDT E Int.*, vol. 31, no. 5, pp. 317–324, 1998.

[66] E. Vannan and P. Vizhian, "Corrosion Characteristics of Basalt Short Fiber Reinforced with Al-7075 Metal Matrix Composites," 2015.

[67] V. V. Rao and C. Ratnam, "Estimation of Defect Severity in Rolling Element Bearings using Vibration Signals with Artificial Neural Network," 2015.

[68] M. Ravan, R. K. Amineh, S. Koziel, N. K. Nikolova, and J. P. Reilly, "Sizing of 3-D arbitrary defects using magnetic flux leakage measurements," *IEEE Trans. Magn.*, vol. 46, no. 4, 2009.

[69] J. W. Bandler, Q. Cheng, D. H. Gebre-Mariam, K. Madsen, F. Pedersen, and J. Sondergaard, "EM-based surrogate modeling and design exploiting implicit, frequency and output space mappings," in *IEEE MTT-S International Microwave Symposium Digest, 2003*, 2003, vol. 2, pp. 1003–1006.

[70] J. W. Bandler *et al.*, "Space mapping: the state of the art," *IEEE Trans. Microw. Theory Tech.*, vol. 52, no. 1, pp. 337–361, 2004.

[71] D. Echeverrĭa and P. W. Hemker, "Space mapping and defect correction," *Comput. Methods Appl. Math.*, vol. 5, no. 2, pp. 107–136, 2005.

[72] S. Koziel, J. W. Bandler, and K. Madsen, "A space-mapping framework for engineering optimization—Theory and

implementation," *IEEE Trans. Microw. Theory Tech.*, vol. 54, no. 10, pp. 3721–3730, 2006.

[73] R. K. Amineh, S. Koziel, N. K. Nikolova, J. W. Bandler, and J. P. Reilly, "A space mapping methodology for defect characterization from magnetic flux leakage measurements," *IEEE Trans. Magn.*, vol. 44, no. 8, pp. 2058–2065, 2008.

[74] J. W. Bandler, S. Koziel, and K. Madsen, "Space mapping for engineering optimization," *SIAG/Optimization Views-and-News Spec. Issue Surrog. Optim.*, vol. 17, no. 1, pp. 19–26, 2006.

[75] N. N. Zatsepin and V. E. Shcherbinin, "On calculation of magnetostatic field generated by surface flaws. I," *Topogr. fields flaws Model. Defektoskopiya*, vol. 5, pp. 50–59, 1966.

[76] F. Förster, "Nondestructive inspection by the method of magnetic leakage fields- Theoretical and experimental foundations of the detection of surface cracks of finite and infinite depth," *Sov. J. Nondestruct. Testing,(ISSN 0038-5492)*, vol. 18, no. 11, pp. 841–858, 1983.

[77] N. N. Zatsepin, V. E. Shcherbinin, and A. M. Pashagin, "Investigation of the Magnetic Field of Flaws on the Inner Surface of Ferromagnetic Pipes. 1," *Basic Regul. Mech. Flaw-f. Form. Defektoskopiya*, no. 2, pp. 8–16, 1969.

[78] V. E. Shcherbinin and N. N. Zatsepin, "Calculation of the magnetostatic field of surface defects. I. Field topography of defect models," *Defectoscopy*, vol. 5, pp. 385–393, 1966.

[79] L. J. Swartzendruber, "Magnetic leakage and force fields for artificial defects in magnetic particle test rings," in *In Proceedings of the XII Symposium on NDE (SWRI, San Antonio, TX)*, 1979, pp. 150–161.